PAPER

Recipes for the fabrication of strictly ordered Ge islands on pit-patterned Si(001) substrates

To cite this article: Martyna Grydlik *et al* 2013 *Nanotechnology* **24** 105601

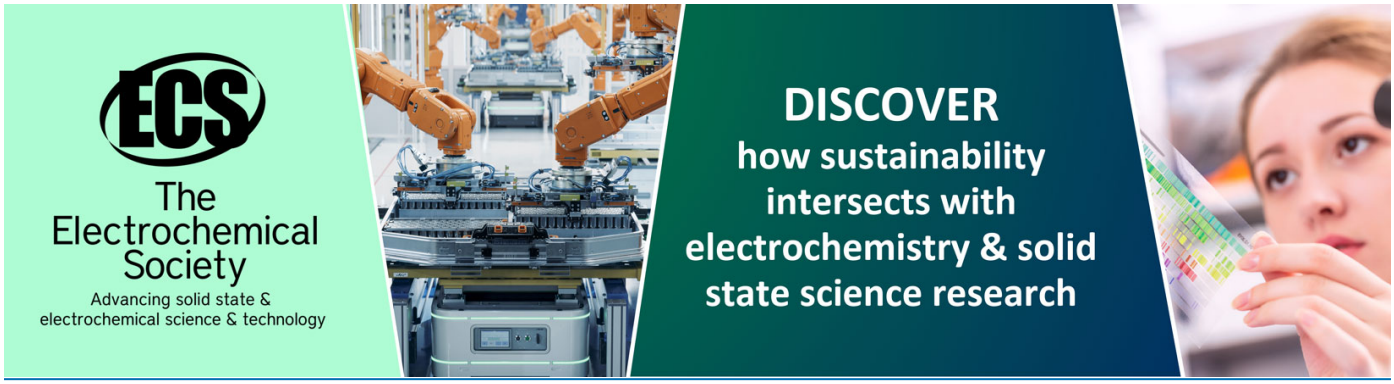

Nanotechnology **24** (2013) 105601 (14pp) doi:10.1088/0957-4484/24/10/105601

Recipes for the fabrication of strictly ordered Ge islands on pit-patterned Si(001) substrates

Martyna Grydlik[1], Gregor Langer, Thomas Fromherz, Friedrich Schäffler and Moritz Brehm[1]

Institute of Semiconductor and Solid State Physics, Johannes Kepler University Linz, Austria

E-mail: brehm.moritz@gmail.com

Received 11 December 2012, in final form 23 January 2013
Published 15 February 2013
Online at stacks.iop.org/Nano/24/105601

Abstract

We identify the most important parameters for the growth of ordered SiGe islands on pit-patterned Si(001) substrates. From a multi-dimensional parameter space we link individual contributions to isolate their influence on ordered island growth. This includes the influences of: the pit size, pit depth and pit period on the Si buffer layer and subsequent Ge growth; the pit sidewall inclination on Ge island growth; the amount of Ge on island morphologies as well as the influences of the pit-size homogeneity, the pit period, the Ge growth temperature and rate on island formation. We highlight that the initial pit shape and pit size in combination with the growth conditions of the Si buffer layer should be adjusted to provide suitable preconditions for the growth of Ge islands with the desired size, composition and nucleation position. Furthermore, we demonstrate that the wetting layer between pits can play the role of a stabilizer that inhibits shape transformations of ordered islands. Thus, dislocation formation within islands can be delayed, uniform arrays of one island type can be fabricated and secondary island nucleation between pits can be impeded. These findings allow us to fabricate perfectly ordered and homogeneous Ge islands on one and the same sample, even if the pit period is varied from a few hundred nanometres to several micrometres.

S Online supplementary data available from stacks.iop.org/Nano/24/105601/mmedia

(Some figures may appear in colour only in the online journal)

1. Introduction

The ordering of Ge quantum dots (QDs), also called islands, on Si substrates [1–24] is a must for any attempt to integrate them into devices based on the existing Si technology, because of the mandatory addressability. Moreover, ordered QDs exhibit improved size uniformity, at least for a larger window of growth parameters [6, 12, 17] and, equally important, their chemical composition is more homogeneous as compared to randomly nucleated islands [14, 15, 17]. Since the chemical composition crucially determines the energy band offsets of the hetero-epitaxial system, the influence of the chemical composition, and its three-dimensional variation within the dots, on the luminescence emission energy is at least as important as the influence of size variations [17].

Accurate control over inter-island distances enables a variety of electronic [25, 26] and optoelectronic applications. Ordered QDs, especially group III–V QDs with type-I band offsets, grown on pit-patterned substrates with pit periods larger than 1 μm can be used for devices with novel functionalities, such as single photon emitters [27, 28], which, in turn, are highly interesting in the emerging field of optical data communications [29]. At the other extreme, when the spacing between the islands enters the nanoscale regime (<100 nm) [12, 16] wavefunctions of the individual

[1] Present address: Institute for Integrative Nanosciences, IFW Dresden, Helmholtzstraße 20, Dresden 01069, Germany.

Table 1. Sample parameters.

Sample group (SG)/sample (S) (# of samples)	Fields	d_{pit} (nm)	Opening diameter (nm)	Depth (nm)	Pit shape
SG_A (2)	7	425	175–425	47–5	Cylindrical
SG_B (2)	7	425–3400	260	45	Cylindrical
SG_C (4)	7	300–900	200	50	Cylindrical
S_D (1)	1	500	200	50	Cylindrical
S_E (1)	1	1000	150–295	106–208	Pyramidal
S_F (1)	1	400	195–225	138–159	Pyramidal

QDs start to interact, and it is expected that mini-bands are formed, similarly to electronic bands in molecules. This would eventually lead to an additional degree of tunability of the electronic and optical properties of the QDs [30, 31]. However, only perfect ordering of the QDs makes their integration into existing devices feasible.

There are several reports describing the effects of individual growth parameters on the growth of ordered Ge islands on Si(001), however, a systematic and concise investigation of this multi-dimensional parameter space has been missing so far. This is what we are aiming at in this contribution. We first give, in section 3.1, a general overview of the most important parameters for the growth of ordered SiGe islands on pit-patterned Si(001) substrates. In the subsequent sections we discuss the following dependences: in section 3.2, the influence of the pit size and depth on the Si buffer layer and on Ge growth; in section 3.3, the role of the pit period on the Si buffer layer growth; in section 3.4, the influence of the pit sidewall inclination on Ge island growth; in section 3.5, the dependence of the amount of deposited Ge on island growth, in section 3.6, the influence of the pit homogeneity on island growth; in section 3.7, the influence of the pattern period and the Ge growth temperature on island growth; and finally in section 3.8, the influence of the growth rate on the Ge wetting layer and Ge island growth.

Since small changes in the composition of the deposited epilayer material usually change the growth in a drastic manner [32–34], also for island growth on pre-patterned substrates [35, 36], we restricted the experiments presented in this work to the deposition of pure Ge on pit-patterned Si only.

The similarities of the Ge on Si(001) system to other hetero-epitaxial systems such as the InAs on GaAs(001) system are highlighted in section 4. Due to this resemblance we believe that many aspects of the growth of ordered Ge islands on pit-patterned Si(001) substrates described in this work can indeed be translated to other material systems such as InAs on GaAs.

2. Fabrication of patterned substrates and island growth

We pit-patterned high-resistivity (>1000 Ω cm) Si(001) substrates by electron beam lithography. Subsequently, the pit pattern was transferred into the substrate either by reactive ion etching (RIE), resulting in approximately cylindrical pits, or by wet etching using tetramethylammonium hydroxide (TMAH), resulting in inverted pyramidal, {111}-faceted pits. The {111}-faceted and the cylindrical pits were fabricated following the method described in [18, 19, 21, 22]. The size of the pit-patterned fields was chosen to be 200 × 200 μm^2 in all cases. We fabricated altogether eleven e-beam-written samples. Their main properties are summarized in table 1. The pits are characterized by their opening diameter, their depth and shape, and finally the distance between individual openings.

For two identical samples (sample group A, (SG_A)) the pit-pattern period (d_{pit}) was set constant to 425 nm on all seven fields, and only the e-beam dose was varied. This resulted, after pattern transfer via reactive ion etching into the Si substrate, in a variation of the pit opening diameter from 175 to 425 nm, while the pit depth varied from 5 to 47 nm. Two other identical samples (SG_B) also contain seven fields, where the pit period was varied from 425 to 3400 nm whereas the pit depths and opening diameters were kept constant for all fields (45 nm and 260 nm, respectively). Four identical samples (SG_C), each containing seven fields with varying d_{pit} from 300 to 900 nm, were fabricated. For those samples the pit depths and opening diameters were 50 nm and 200 nm, respectively. Additionally, sample (S) D (S_D) had one single field with 500 nm pit period and the cylindrical pits had a depth and diameter of 50 nm and 200 nm, respectively. One sample, S_E had a single field with $d_{pit} = 1$ μm and wet-etched, pyramidal {111}-faceted pits with different opening sizes, ranging from 150 to 295 nm. Similar {111}-pits with slightly irregular opening sizes were produced on sample S_F, where d_{pit} was chosen to be 400 nm.

The samples were cleaned *ex situ*, and immediately before their introduction into a load-lock chamber received a dip into diluted (1%) hydrofluoric acid (HF) to remove the natural oxide. Growth was carried out in a Riber Siva 45 solid source molecular beam epitaxy (MBE) facility. After *in situ* degassing at 700 °C for 40 min, we grew on *all samples* a Si buffer layer by depositing 45 nm of Si at a rate of 0.6 Å s^{-1} and at a growth temperature that was ramped up from 450 to 550 °C. The buffer layer step was finished by a ramp-up step to the respective growth temperature of Ge (T_{Ge}), during which both the Ge and the Si shutter were closed. On one of the two samples of each group SG_A and SG_B three monolayers (ML) of Ge were deposited at $T_{Ge} = 700$ °C (rate: 0.03 Å s^{-1}), whereas for the other sample of each of these groups the growth sequence was stopped before the Ge deposition, i.e. after the Si buffer growth and the subsequent ramp-up to T_{Ge}.

For SG_C we chose T_{Ge} to be 650 °C, 690 °C, 725 °C and 760 °C, respectively. For all samples in SG_C, 6 ML of Ge

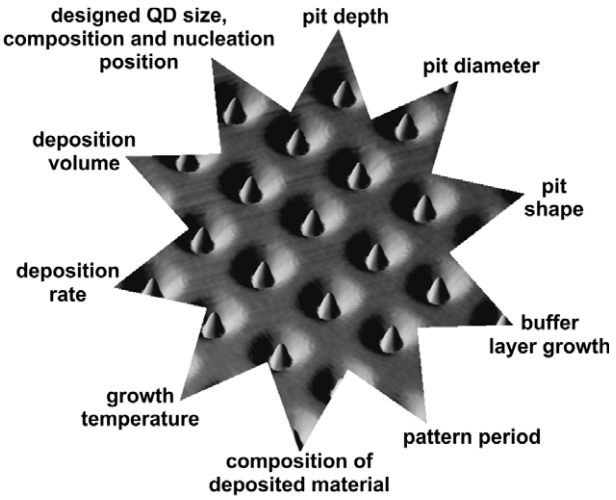

Figure 1. Parameter space for strictly ordered island growth on pit-patterned substrates, linking the most important factors for the growth of strictly ordered Ge/Si quantum dots on pit-patterned Si(001) substrates.

were deposited at a growth rate of 0.05 Å s^{-1}. For samples S_D ($d_{pit} = 500$ nm), S_E ($d_{pit} = 1000$ nm) and S_F ($d_{pit} = 400$ nm), 6 ML, 3.8 ML and 5 ML of Ge were deposited at $T_{Ge} = 625\,°C$, 700 °C and 700 °C, respectively.

After growth, the surface of the samples was characterized *ex situ* using a Digital Instruments Dimension 3100 atomic force microscope (AFM) with sharpened Si tips having half-opening angles of 15° and nominal tip radii of 2 nm.

In the following sections most of the AFM micrographs are presented in the surface-angle image (SAI) mode, where the local surface slope is plotted with respect to the (001) substrate surface. The colour coding was chosen in such a way that stable facets can be immediately identified by different colours (for more information on this nano-goniometric method see [37]).

3. Results and discussion

3.1. Conditions for perfect ordering of QDs in the Ge/Si system

In order to obtain both perfect ordering of islands and also structural and optical properties, many aspects of substrate patterning and growth have to be taken into account. A summary of the ten most important parameters for the growth of ordered Ge islands on pit-patterned Si(001) substrates is depicted in figure 1. Depending on the respective application, QDs of different size and chemical composition are desired.

Therefore, as summarized in figure 1, the designed QD size and chemical composition, desired nucleation position (in the pit or at certain positions at the pit rim), pit depth, pit diameter and pit shape, Si buffer layer growth, pattern period, composition of the deposited material, growth temperature, deposition rate and volume have to be adjusted in order to get optimal growth conditions. Besides this multi-dimensional parameter space, there are additional preconditions that need to be fulfilled for the growth of strictly ordered SiGe island ensembles. For example, the substrate type and orientation [38] has to be adjusted to the designed QDs. No contamination or crystalline defects should be introduced during the fabrication of the pit-patterned templates. The sample surface has to be perfectly clean and surface roughness on the planar parts between the pits has to be avoided by any means to ensure large enough surface diffusion lengths for the deposited adatoms.

Usually, samples are degassed *in situ* at an elevated temperature before the material deposition steps. This procedure ensures that hydrogen atoms and other possible remaining surface impurity molecules can be desorbed before the Si buffer layer is grown. The degassing step has to be performed below a temperature of about 750 °C in order to prevent the formation of silicon carbide and changes of the original pit shape [18]. Also a complete removal of the native SiO_2 by a HF dip turned out to be extremely important, since any remaining SiO_2 induces a large Si atom mobility beneath the SiO_2, resulting in a complete smearing out of the Si pits during the degassing step [39].

3.2. Influence of the pit size/depth on the Si buffer layer and on Ge growth

The Si buffer layer serves two purposes: first, it should provide an epitaxial layer that acts as a separation layer between the QDs and the initial substrate surface and possible impurities therein. Second, it should convert etched pits into smooth shapes defined by low-surface-energy facets of the respective material system. The latter often leads in the case of Si pits to inverted pyramids with {11n}-facets and $n > 7$ form [10, 11]. One probable reason for the success in growing ordered Ge QDs on Si(001) pit-patterned substrates as compared to other material systems is that strained Ge develops the low-energy {105} facet, which is inclined at 11.3° to the substrate surface. Its angle is close to those of the {117} to {1 1 10} facets (inclined at 11.4°–8° with respect to the surface plane) that can be formed during Si buffer layer growth on the pit-patterned substrate [7, 9–11].

Several reports describe the evolution of the pit shape after the growth of a Si buffer layer [7, 9–11], but only for a few selected pit periods and initial pit dimensions. Since the Si buffer layer growth is a key to the successful growth of ordered islands on pit-patterned substrates, a systematic correlation of the original pit dimensions and the pit period with Si buffer layer growth is given next.

As mentioned in section 2, we can separate the influence of the pit dimensions and periods by writing a matrix of patterned fields on a single Si(001) substrate, where for example along the matrix columns (rows) the pit dimensions (pit periods) are varied. In this way, all fields of the matrix undergo the same processing and growth conditions.

In panels (a)–(g) of figure 2, the sub-panels (i) show AFM micrographs of pits on sample SG_A before Si buffer growth. The colour coding contains the depth information of the pits. The black lines in figure 2(h) show the corresponding line scans in the [110]-direction through the middle of the pits, which before growth have different opening diameters ranging

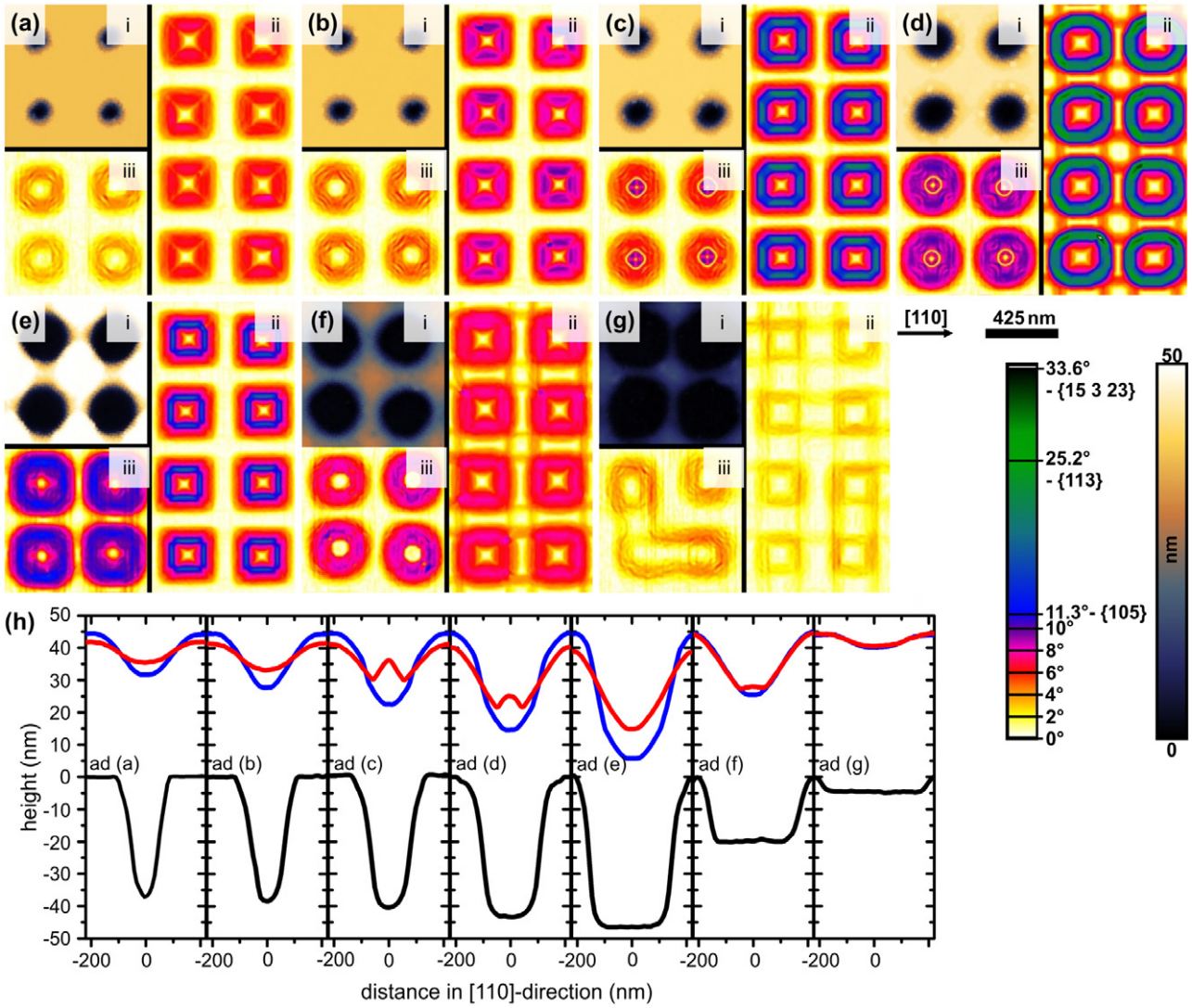

Figure 2. Influence of pit dimensions on the Si buffer layer and Ge growth. Sample group SG_A. For all fields $d_{pit} = 425$ nm. (a)–(g) Sub-panels (i): AFM images of the pits before growth. The colour coding contains the depth information of the pits. The pit diameters before growth are (a) 175 nm, (b) 212 nm, (c) 262 nm, (d) 292 nm, (e) 344 nm, (f) 420 nm and (g) 425 nm. (a)–(g) Sub-panels (ii): Surface inclination images (SAI) of the respective pits shown in sub-panel (i) after growth of a 45 nm thick Si buffer layer. The colour coding was chosen in such a way that for inclinations $<10°$ the colour changes (from white to violet) every 2°, see left colour bar. Additionally, the stable Ge and SiGe facets {105} (11.3°), {113} (25.2°) and {15 3 23} (33.6°) are indicated by their own colour, blue, green and black, respectively. (a)–(g) Sub-panels (iii): SAIs of the respective pits shown in sub-panel (ii) after the deposition of 3 ML of Ge at 700 °C. (h) Linescans in the [110]-direction through the middle of the pits shown in (a)–(g) before growth (black curves), after Si buffer layer growth (blue curves), and after Ge growth (red curves).

from 175 to 425 nm (see also figures 2(a)–(g)). The pits were etched by RIE in one and the same etching step since all fields are located on one sample. However, because of geometrical limitations of the AFM tip (see section 2), the measured pit depths are slightly lower for pits with smaller opening sizes (see figure 2(h)). For the pits with opening sizes larger than 344 nm, shown in figures 2(f) and (g), the pit depth decreases to 20 nm and 5 nm, respectively, since the RIE etching also begins to attack the sidewalls between the pits. This happens because the resist (in this case e-beam resist) does not have a sharp edge in close proximity to the pit, but is slightly rounded. In the case of pits nearly touching each other, this lithographic imperfection can lead to an eventual merging of the pits during etching. For the AFM line-scan analysis (figure 2(h)), we set the zero level in such a way that the (001) surface outside the patterned fields is at the same height of 47 nm.

In the sub-panels (ii) of figures 2(a)–(g), AFM surface-angle images (SAI, see also [37, 40]) after Si buffer layer growth (45 nm at a substrate temperature ramped up from 450 to 550 °C) are shown. The colour coding was chosen in such way that for facet angles in the range between 0° and 10° the colour changes when the angle changes by 2°. Additionally, the colours blue, green and black indicate the well-known Ge and SiGe facets {105}, {113} and {15 3 23}, respectively. Such a colour coding makes it easy to distinguish between differently faceted pits, even if most of them are of inverted pyramidal shape [7, 9–11] or—at least in their

cross-section—inverted bell-like shape (see blue linescans in figure 2(h)). After buffer layer growth the maximum pit sidewall inclination changes to ∼6° for an initial pit diameter of 175 nm (figure 2(a), panel (ii)), and to 33.6° for an initial pit diameter of 292 nm (figure 2(d), panel (ii)).

If not limited by the pattern period, the pits after Si buffer layer growth are in general shallower but wider, as already reported in [7, 9–11]. In the sub-panels (iii) of figures 2(a)–(g), we present SAIs of the pits after the deposition of the Si buffer layer and subsequent growth of 3 ML of Ge at $T_{Ge} = 700\,^{\circ}C$. As evidenced in figure 2, Ge deposition further smoothens the pits and the respective steepest pit sidewall inclination angles are further reduced. This so-called anomalous smoothening effect is theoretically explained in [41]. Pyramidal islands (figures 2(c) and (d), sub-panel iii) are observed in pits with sidewall angles between 5° and 7° (figure 2(c)), and 8° and 11° (figure 2(d)).

It is important to mention that the relative positions of the line scans shown in figure 2(h) with respect to each other were estimated on the basis of the amount of deposited Si and Ge and the conservation of volumes. The real respective positions of the line scans can probably only be clarified by cross-sectional transmission electron microscopy experiments. However, we are confident that the positions calculated from volume conservation as shown in figure 2(h) are close to reality.

Summarizing the results presented in figure 2, it becomes evident that the smoothening of the pits by the Si buffer layer that takes place via surface faceting by {11n}-facets such as {113}-facets results in inverted pyramidal and bell-shaped pits after Si buffer layer growth. There is obviously no specific stability of the pits against capillary forces driving the surface smoothening [42], which, in turn, emphasizes the importance of adjusting the growth parameters of the Si buffer layer to the initial pit dimensions, since perfectly ordered islands with homogeneous size distribution can only be grown in pits with certain properties, as will be described in detail in section 3.4.

3.3. Influence of the pit period on Si buffer layer growth

It was not evident *a priori* whether for identical pits an area increase of the planar parts between the pits, i.e. an increase of d_{pit}, would influence the pit shape during Si buffer layer growth. In general, with increasing d_{pit} more deposited material is available per unit cell of the pattern, which could be driven into the respective pit by capillary forces [42]. Thus, for SG_B we fixed the original pit opening diameter and depth to 260 nm and 45 nm, respectively, and varied only the pattern period to determine its influence on the pit shape after Si buffer layer growth. Figures 3(a) and (b) depict pits after buffer layer growth for periods of 850 and 3400 nm. Additionally, figure 2(c), sub-panel (ii) (sample SG_A), shows pits with a period of 425 nm and an original pit diameter of 260 nm. From the SAI images, and also from the statistical evaluation of the most important pit parameters (i.e. depth, diameter, and volume), presented in figure 3(c), it becomes clear that the pattern period has only a slight direct influence on the morphological evolution of the pits during buffer layer

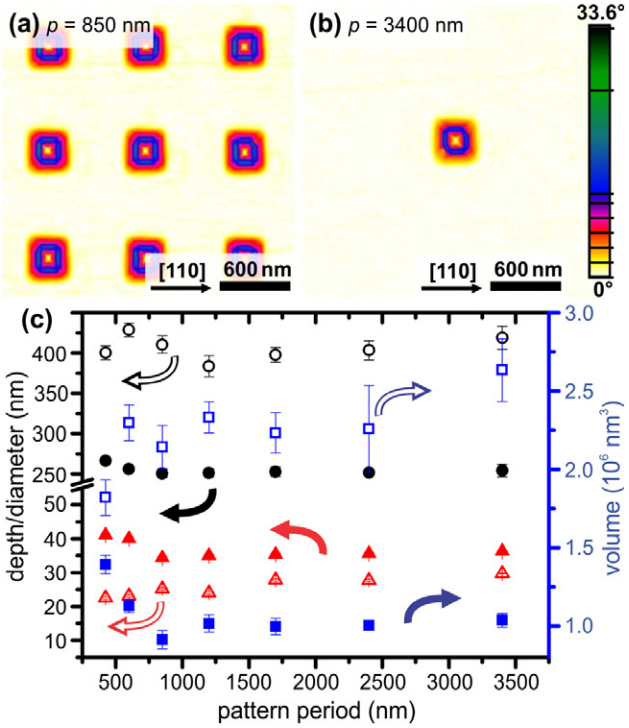

Figure 3. Influence of pit-period on Si buffer layer growth for substrate template SG_B. (a) and (b)AFM–SAI of pits (original pit depth and diameter: 45 and 260 nm) with (a) $d_{pit} = 850$ nm and (b) $d_{pit} = 3.4\ \mu$m. (c) Statistical evaluation of the pit depth, diameter and volume performed on 30 pits per period. The full symbols describe the pit before growth and the open symbols after growth. Red triangles describe the pit depth, black circles the diameter and blue squares the volume. The open and full arrows point to the respective ordinate.

growth, i.e. the pit depths, diameters and volumes after Si deposition do not vary with increasing d_{pit}. We attributed this behaviour to the relatively low surface mobility of Si as compared to Ge [43], which is related to a larger Si–Si adatom binding energy as compared to the Ge–Ge case. The observed virtual independence of the Si buffer properties from d_{pit} is in strong contrast to the influence of d_{pit} and the amount of Ge deposition on Ge island growth, as will be explained in section 3.7. It can be seen from figure 3 that, in general, the pit depth decreases with Si buffer layer deposition, while the pit diameter as well as the volume increases, i.e. the pits become shallower and wider (see also [7, 9–11] and figure 2).

3.4. Influence of pit sidewall inclination on Ge island growth

The sidewall angle of the pits after the growth of the Si buffer layer and the Ge wetting layer has a substantial influence on the nucleation position of Ge islands. In a recent work [19] we have shown that the pit sidewall angle (α_{pit}) has to be lower than 30° to make island nucleation inside the pit energetically favourable. In contrast, for $\alpha_{pit} > 30°$, relaxation of the strain accumulated in the substrate and the initial relaxation of the wetting layer favour island nucleation at the rim of the pits [19, 44, 45]. The morphological evolution during the growth of such rim-bound islands can be found in [46]. There

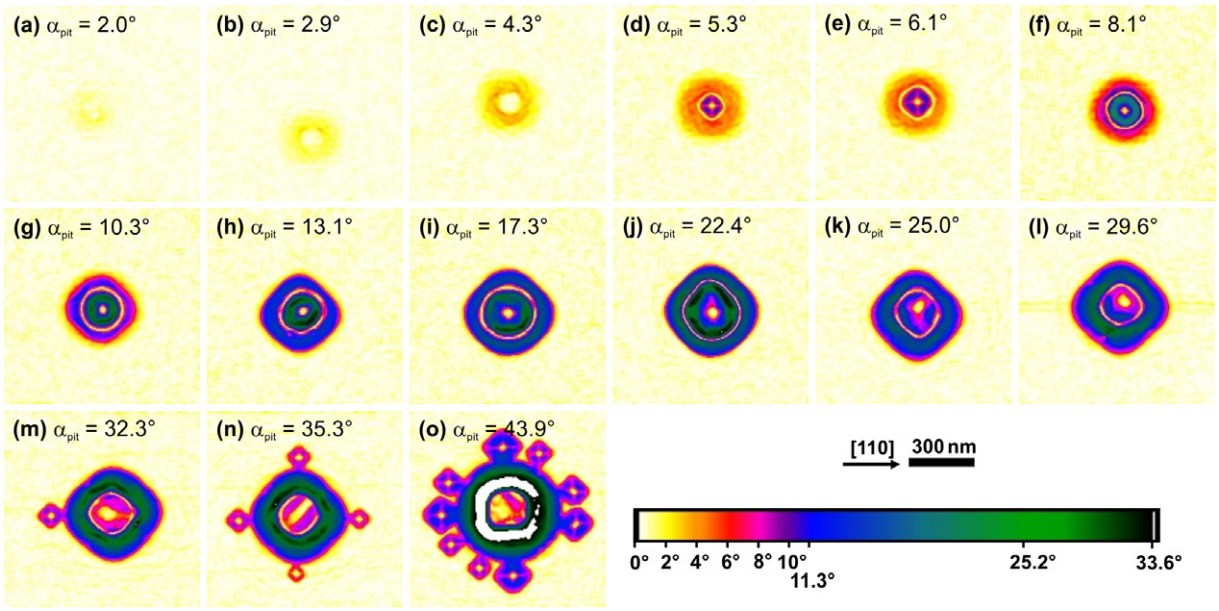

Figure 4. Influence of pit sidewall angle on Ge island growth I. AFM–SAI images of sample S_E. (a)–(o) Originally {111}-pits with $d_{pit} = 1$ μm and varying opening size (150 nm for (a) and 295 nm for (o)) after Si buffer layer growth and deposition of 3.8 ML of Ge at 700 °C. For none of the pits with $\alpha_{pit} < \sim 5°$ island formation is observed in the pit. (See also figures 2(a) and (b), panels iii), while for $\alpha_{pit} > \sim 30°$, in (m)–(o), islands nucleate at the rim of the pit. Only for $\sim 5° < \alpha_{pit} < \sim 18°$ highly symmetric islands grow in the middle of the pits.

it is shown that the influence of the pit leads to additional tweezers-like faceting of the pre-pyramids and pyramids.

Figures 4(a)–(o) show pits (S_E) with different sidewall inclination angles, produced by the method described in [19]. The differently sized pits were initially of {111}-faceted pyramidal shape. After the growth of the buffer and the Ge wetting layer we obtained, depending on their initial size, pits with varying sidewall inclination angles ranging from 2° to 54.7°. Figure 4 demonstrates that island formation occurs only for pits with $\alpha_{pit} > \sim 5°$, whereas for lower α_{pit} it seems to be energetically favourable to flatten the already very shallow pits, instead of nucleating upright islands. We found for all sample groups (see also section 3.6) that islands do not nucleate inside or around pits, if the pits are too shallow, i.e. if $\alpha_{pit} < \sim 5°$. We find that $\sim 5° < \alpha_{pit} < \sim 18°$ represents the optimum pit sidewall inclination angle window for which highly symmetric islands grow at the centre of the pits (see figures 4(d)–(i)). Thus, this sidewall inclination angle region is of greatest interest for most applications.

For steeper pit angles $\sim 18° < \alpha_{pit} < \sim 30°$ (figures 2(j)–(l)) the islands in the pit centre tend to be asymmetric and the island facets become shallower. Upright Ge islands forming in such pits are in an intermediate state where the nucleation position in the middle of the pit becomes less favourable [19].

Finally, for $\alpha_{pit} > \sim 30°$, islands start to nucleate at the rim of the pit for the aforementioned reasons.

In figure 5 we present a borderline case (sample S_D), where the pit sidewall inclination angle is about 26°, and thus rim-bound pyramids (P_{rim}) co-exist with pyramids (P_{pit}) and domes nucleating inside the pits (D_{pit}). Additionally, also asymmetric, dislocated islands called superdomes (SD) [47]

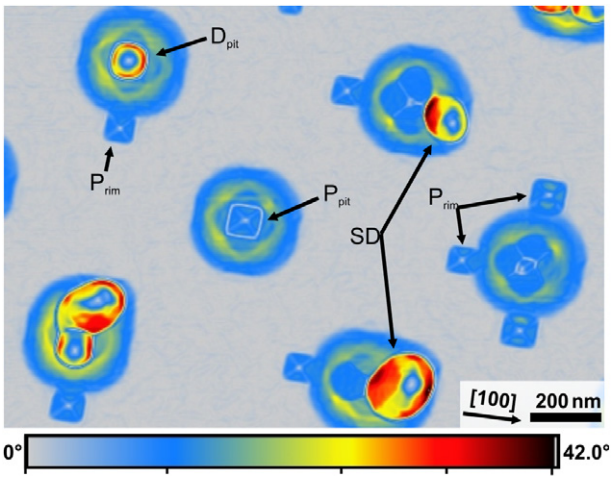

Figure 5. Influence of pit sidewall angle on Ge island growth II. AFM micrograph in SAI mode of a pit-patterned sample after deposition of both the Si buffer and Ge on sample S_D, 6 ML of Ge grown at 625 °C, $d_{pit} = 500$ nm. α_{pit} is between 25° and 30° (yellow colour) and thus represents the limiting pit shape for nucleation inside the pit (domes and pyramids, D_{pit} and P_{pit}, respectively) and nucleation at the rim of the pit (P_{rim}). The colour bar is chosen in such a way that the {105}-facets (blue), {113}-facets (yellow) and {15 3 23} (red)-facets have their own colour.

can be found in some of the pits since the pit sidewall inclination angle is not perfect for either island configuration (rim, or middle of the pit).

A general trend for perfectly ordered island growth in the middle of pits seems to be the following: (i) the pit sidewall angle should be between 5° and 18° (see discussion above) and (ii) the ratio between the island diameter and the pit

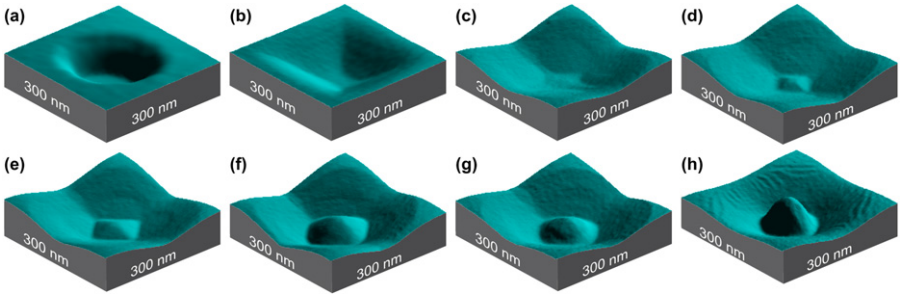

Figure 6. Island evolution with increasing Ge coverage per unit cell area. 3D-AFM micrographs of a pit (a) before growth, (b) after Si buffer layer growth, (c)–(h) with increasing Ge deposition at $T_{Ge} = 650\,^{\circ}C$. With an increasing amount of Ge per 300×300 nm^2 unit cell area (6 ML for (c) and 10 ML for (h)) the evolution from pit faceting (c) to the formation of pyramids (d)–(f), transition domes, and domes (h) can be followed.

diameter after Ge growth has to be around 1:2. This was certainly verified for the samples investigated in this work, but also for very small dots of 3 nm height and 35 nm base diameter that are located in about 70 nm wide pits [48], as well as for very large but still coherent islands (diameter about 300 nm) that are grown in the middle of 500 nm wide pits [49].

3.5. Influence of the amount of deposited Ge on island growth

On a coarse scale concerning the deposited Ge volume, it is evident that the deposition volume plays a crucial role, since beyond a critical thickness strained epilayers inevitably relax by the formation of unwanted misfit dislocations [50]. On a much finer scale more subtle effects play a role. Island formation on planar substrates occurs at a Ge coverage of around 4.2 ML on Si(001) [51, 52]. However, before islands are nucleated, the wetting layer (WL) grows to an overcritical thickness as a consequence of the lower surface energies of the epilayer material (Ge) as compared to the substrate material (Si) [53, 54]. Islands in pits, on the other hand, can only grow to a certain volume before they eventually start to introduce dislocations [22]. Thus, if the deposited material exceeds the volume that is needed to achieve a critical WL thickness plus the material that is needed to form the islands in the pits, secondary island nucleation will take place between the pits [9, 21, 55].

The influence of the pattern period is strongly correlated with the amount of deposited material, since every pit is surrounded by a unit cell area (i.e. the pit-period squared) from which mobile Ge atoms can be statistically collected by the pit. Thus, for large pit periods less material has to be deposited to form QDs of the same size than for small pit periods [16, 21].

On a flat substrate, and for elevated growth temperatures above about 670 °C, dome islands are the first stable species growing on a metastable WL before pyramids appear [51, 52]. On pit-patterned substrates the situation is different. The WL does not tend to grow to an overcritical thickness [20] since the pits act as material sinks that attract the loosely bound Ge in the third and fourth monolayer. Since an overcritical thickness, metastable WL is not present between the pits, initial dome formation prior to pyramid formation in the pit is neither expected nor observed experimentally.

Figures 6(a) and (b) present a pit before and after Si buffer layer growth, where the previously discussed faceting of the pit with Si buffer growth can be seen. The pit period is in this case 300 nm. Figures 6(c)–(h) depict the island evolution from WL faceting (figure 6(c)) to small and larger pyramids [56] (figures 6(d)–(f)), transition domes [57, 58] (figure 6(g)), and domes [59, 51] (figure 6(h)). During the AFM micrograph sequence shown in figures 6(c)–(h) the amount of Ge per 300×300 nm^2 pattern unit cell increases from 6 to 11 ML. The whole morphological evolution of one Ge dot in a pit with increasing amount of Ge deposition can be seen in Video 1 in the supplementary material (available at stacks.iop.org/Nano/24/105601/mmedia), where single AFM micrographs are linked together to form the movie.

This difference in the growth-morphology evolution, as compared to Ge island growth on planar substrates, is of importance since it allows, on patterned samples, the growth of an array of small pyramids, a few nm high, without the existence of larger domes (see section 3.8).

3.6. Influence of the pit homogeneity on island growth

It is not too surprising that for strictly ordered island growth the initially fabricated patterned pits need to be highly homogeneous in their structural dimensions. Here, we demonstrate that even very small pit-size inhomogeneities of less than 4% of the pit-opening lengths can have a drastic influence on the growth of Ge islands. Figure 7(a) depicts an AFM height image of the sample with wet-etched (in TMAH), {111}-faceted pits ($d_{pit} = 400$ nm) before the growth (S_F). Due to temporary problems with the e-beam lithography system, the pits were inhomogeneous in size (see figure 7(a)). The standard deviations, based on measurements of 34 pits, are 4.3% in pit depth and 7.4% in pit-opening area. This otherwise undesired pattern fluctuation was exploited here to investigate the influence of the relatively small pit-size variation on island growth. Figure 7(b) depicts the sample after the growth of 5 ML of Ge, deposited at $T_{Ge} = 700\,^{\circ}C$, in an AFM micrograph in SAI mode. The deposition of the Si buffer layer and of the 5 ML Ge lead to single islands located off-centre, as well as to double and triple islands in the pits. Apparently, pits with small α_{pit} do not lead to the nucleation of islands, see figure 7(b), which is in agreement

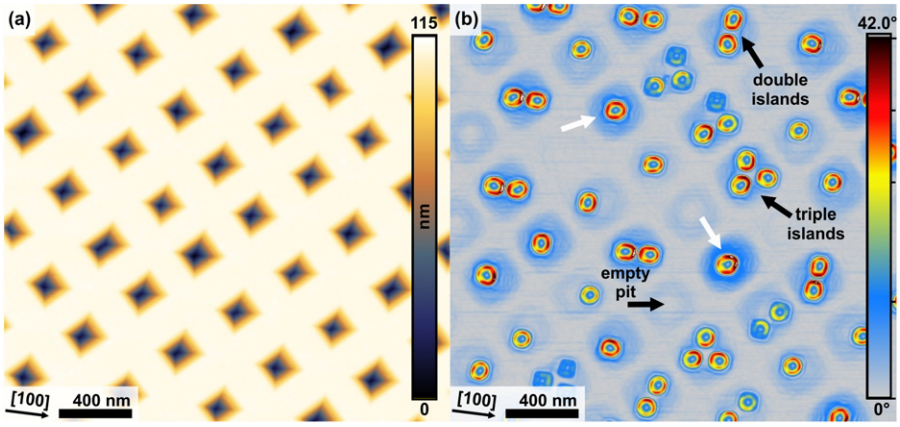

Figure 7. Influence of the pit homogeneity on Ge island growth. Sample template S_F: (a) AFM height mode image of the {111}-pits ($d_{pit} = 400$ nm) before growth. The pit dimensions are inhomogeneous due to defective e-beam lithography. (b) AFM micrograph in SAI mode. 5 ML of Ge were deposited at 700 °C. The Si buffer layer and Ge layer growth lead to single dots located off-centre, as well as double dots and triple dots in the pits. Pits with small α_{pit} do not host islands, while nicely centred islands are only found in steeper pits (dark-blue colour—see white arrows).

with the findings of section 3.4 (figure 4). Islands positioned in the centre of a pit are only found in steeper pits with $\sim 5° < \alpha_{pit} < \sim 18°$, as discussed in section 3.4 (dark-blue colour—see white arrows in figure 7(b)).

3.7. Influence of pattern period and Ge growth temperature on Ge island growth

The Ge growth temperature plays a significant role when designing dot shapes and material compositions, since the degree of intermixing of the QDs with the underlying substrate [22, 60, 61] is correlated with the growth temperature. This affects the effective lattice mismatch of the dots and also the band offsets, and thus the emission properties of the QDs [62]. The effect of the growth temperature on the diffusion of the adatoms is not a major bottleneck when designing perfectly ordered dots, since for not too low MBE growth temperatures (>600 °C) the diffusion length of Ge is at least an order of magnitude larger than the pit periods used within this work [55, 63].

Figure 8 summarizes the influences of the pattern period d_{pit} and T_{Ge} on the island morphology and their nucleation position. For all samples, 6 ML of Ge were deposited at a rate of 0.05 Å s^{-1}. For all T_{Ge} one can find periods in the range 300–400 nm for which single islands nucleate exclusively in the pre-patterned pits (see e.g. figures 8(a), (d), (g) and (j)). Depending on T_{Ge} and d_{pit}, those islands are either pyramids (P_{pit}), domes (D_{pit}), or transition states (transition domes TD_{pit}). For a high Ge growth temperature of 760 °C, the pits in which the islands are located after Ge growth are shallower than the ones where Ge was deposited at lower T_{Ge}. In figures 8(j)–(l) this can be seen from the light blue colour, whereas the corresponding pits in figures 8(a)–(i) are darker, i.e. steeper. As discussed in section 3.6 (see figure 7(b)), if pits are too shallow, then islands tend to nucleate not at the centre of the pit, but rather on the sides of the pit. This trend can also be followed in figure 8(k).

For higher d_{pit}, the ratio between the area of the flat regions between the pits and the area of the pits increases. Thus, the relative amount of Ge that can be transferred to a pit, and thus contribute to island growth there, increases. Depending on the growth rate (see section 3.8), this can lead to the formation of large dislocated superdomes (SD) [21] and double occupation of islands in the pits, as well as a thickening of the WL between the pits [21]. In the latter case secondary island nucleation sets in once the critical WL thickness for island formation is reached in the flat substrate regions between the pits. Superdome formation and the formation of secondary islands are unwanted for any kind of application, since the former leads to a strong quenching of photoluminescence emission from the island ensemble [21] and the latter spoils the addressability and homogeneity of the islands.

Thus, we will describe, in the following, strategies to achieve perfect control over island growth without superdome and secondary island formation for a large range of pit periods.

3.8. Influence of Ge growth rate on Ge island growth

The Ge deposition rate plays a crucial role for uniform island nucleation. For the right combination of pit size and shape (as discussed above) quantum dots nucleate inside the pits, which act as preferential nucleation sites. Triggered by differences in the chemical potential, the deposited Ge flows towards the pits [1] via surface diffusion effects. If the growth rate is too high, the material stored in the WL around the pits is very quickly buried by the next epilayer of atoms. For instance, if the deposition rate is about 0.1 ML s^{-1}, then one layer is fully buried after 10 s by the next arriving layer. For the growth rates used in this work, which are typical for ordered Ge island growth [6, 8, 10, 11, 17, 20, 21], Ge atoms can diffuse tens of microns on the substrate and the wetting layer surface before they are incorporated [55, 63]. Pits and islands attract diffusing Ge atoms with a certain, island-specific capture rate [55]. The lifetime of a single Ge atom on a Ge wetting layer is on the order of tens of

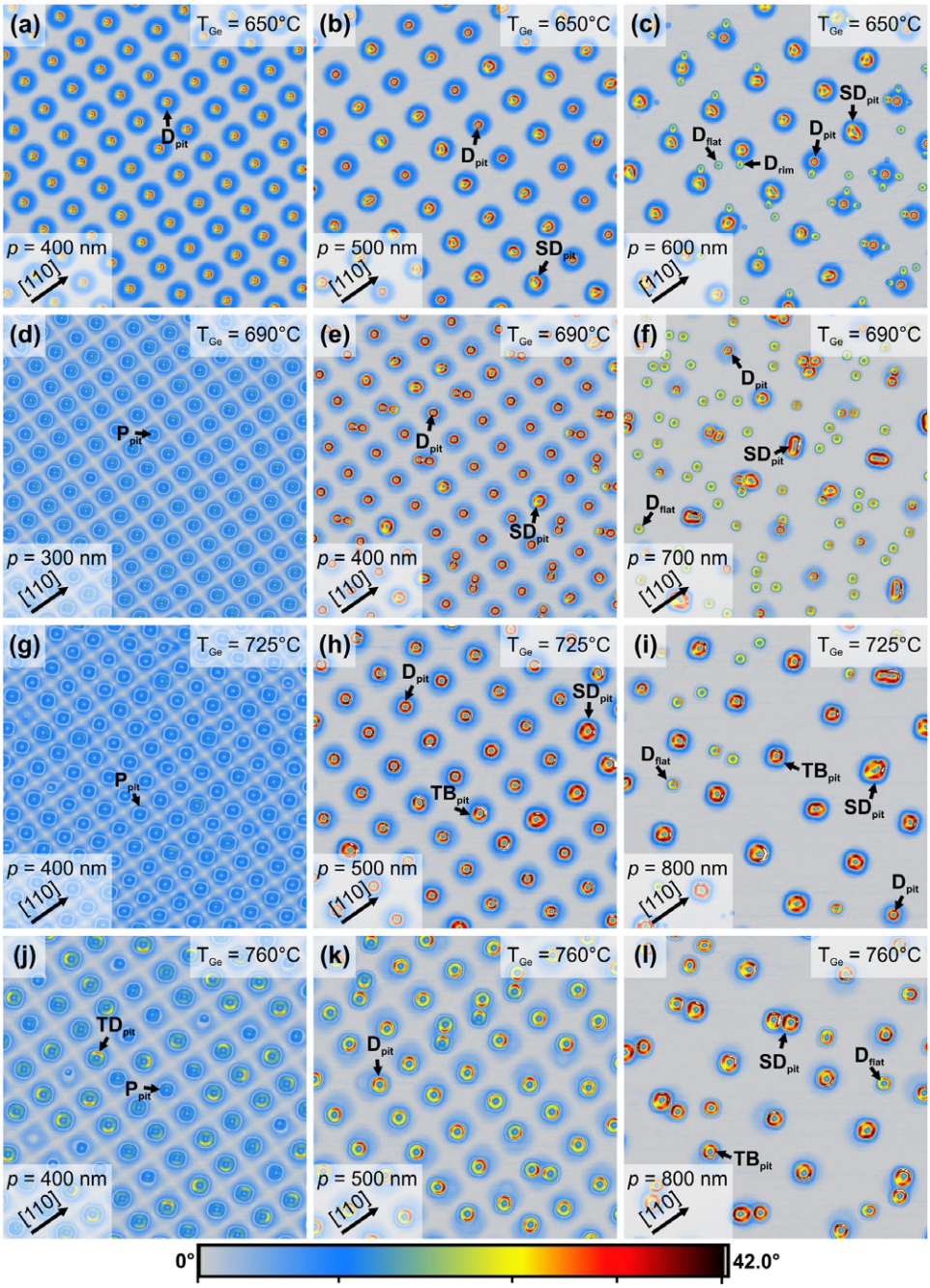

Figure 8. Influence of the pattern period and T_{Ge} on island growth. AFM micrographs in SAI mode of SG_C. The colours blue, yellow and red correspond to {105}, {113} and {15 3 23}-facets, respectively. 6 ML of Ge were deposited at (a)–(c) 650 °C, (d)–(f) 690 °C, (g)–(i) 725 °C and (j)–(l) 760 °C. Islands (pyramids P_{pit}, domes D_{pit}, transition domes TD_{pit}, transition barns (T_B—facets: {105}, {113}, {15 3 23}, {20 4 23} and {23 4 20}) and superdomes SD_{pit}) nucleate in the pits for $d_{pit} < 600$ nm. (c), (f), (i), (l) For $d_{pit} > 600$ nm secondary islands nucleate on the flat regions between the pits.

seconds before it is incorporated into the WL or an island [55]. Thus, it is necessary to choose a growth rate not too large in order to allow material flow towards the pits. Otherwise, the adatoms that cannot reach the pits before they are buried by the next arriving monolayer become trapped in the planar areas between the pits, and therefore lead to a thickening of the WL. At its critical thickness of ∼4.2 ML, secondary islands start to nucleate between the pits [21].

Figure 9 schematically shows the balance between incorporation rate (red arrows) and deposition rate (green arrows). In the example presented in figure 9(a) the incorporation rate is larger than the deposition rate, hence islands nucleate only in the pits. For larger pit-periods, figure 9(b), the incorporation rate is lower than the deposition rate, because of the lower density of material sinks. If this is the case, then part of the deposited material will contribute to a thickening of the WL between the pits and, eventually, lead to island formation there, as shown in the right panel of figure 9(b) and experimentally observed in figures 8(c), (f), (i) and (l).

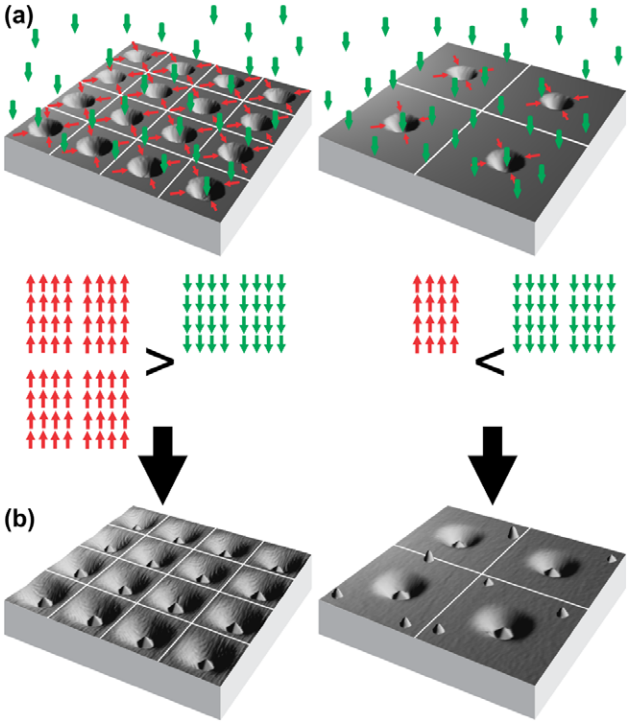

Figure 9. Influence of deposition and incorporation rate on the location of island nucleation. Schematic representation of a pit-patterned substrate with small and large d_{pit} but otherwise identical pit dimensions. Every pit collects randomly Ge atoms from the surroundings with a specific capture rate indicated by red arrows. The deposition rate is indicated by green arrows. If the incorporation rate (number of red arrows) is equal to or higher than the deposition rate (number of green arrows) then islands nucleate only on their favourable position (in the pit for rather flat pits (inclination angles between 5° and 18°)). Otherwise, secondary island nucleation on the flat areas between the pits is unavoidable, once the WL there exceeds its critical thickness of ∼4.2 ML.

Therefore, two conclusions for the growth of islands on pit-patterned fields with large d_{pit} can be drawn: first, the growth rate must not be too high in order to allow an effective Ge transfer to the material sinks (pits) before the adatoms get covered by the next deposited layer. Second, even for very low growth rates, when the number of material sinks approaches zero (i.e. very large pit periods of several micrometres), island formation on the flat regions is unavoidable if the amount of deposited Ge is so high that the WL between the pits reaches the critical thickness for island formation (4.2 ML for $T_{Ge} = 700\,°C$, [51]). Thus, to obtain strictly ordered islands on substrates with large d_{pit}, one has to deposit an amount of Ge that would be below the critical thickness (4.2 ML), but above 3 ML, since below this thickness atoms are very strongly bound in the WL [53, 54], which prevents Ge diffusing to the pits. For amounts of 3–4.2 ML the Ge atoms in the topmost layers are, due to their lower surface energy [54], only weakly bound and will contribute to island growth in the pits.

Figure 10 presents perfectly ordered pyramids for d_{pit} varying from 425 (figure 10(a)) to 3400 nm (figures 10((g), (h))). Note that *all* these fields were located on one and the same sample (SG_B) and, thus, were grown in the same MBE growth run under the aforementioned growth conditions, i.e. 3 ML of Ge were grown at $T_{Ge} = 700\,°C$ and at a growth rate of 0.03 Å s^{-1}.

Figure 11 reports the measured volumes of the islands depicted in figure 10 (empty red squares) and the WL thickness between the pits versus the unit cell area (i.e. d_{pit}^2). Since the surface area of the pits, the amount of deposited Ge per pattern unit cell area and the average Ge content in the islands (about 42% at $T_{Ge} = 700\,°C$ [22]) are known, and the island volume can be determined by AFM analysis, it is possible to estimate the WL thickness in the flat regions between the pits for every d_{pit}. The uncertainties in the exact amount of deposited Ge are smaller than about ±4% for the MBE system used and ±2.5% in the Ge content of the islands [22]. However, the largest uncertainty remains the amount of Ge collected by the pit *before* the pyramid evolves. Zhang *et al* [11] report that for similar growth conditions pre-pyramids in pits only start to form after the deposition of ∼3.7 ML of Ge. In [55], we show that for lower Ge growth temperature (650 °C instead of 700 °C used in this work) but similar pit size, 6 ML of Ge are stored in the pit before islands start to grow. Based on selective wet-etching experiments, Zhang *et al* [20] qualitatively demonstrate that for a Ge deposition of 3.5 ML (i.e. before island formation) Ge is indeed transferred from the planar parts between the pits to the pits. Hence, it is reasonable to assume that the WL in the pits is thicker than between the pits, but a quantitative determination of the differences in the respective WL thickness is difficult to extract.

Thus, we have calculated the WL thickness between the pits for three cases: As an example we assumed that 2.8 ML of Ge (full green circles), 3.3 ML of Ge (full blue stars) and 3.8 ML of Ge (full black squares) contribute to the initial pit faceting (see figure 11).

While for the larger d_{pit} in all three cases the WL thickness approaches 3 ML (for $d_{pit} = 3.4\ \mu m$, only 0.4% of the deposited Ge per unit cell is stored in islands) we find that for the smaller pit periods the remaining WL thickness is significantly smaller. For $d_{pit} = 425$ nm almost 19% of the deposited Ge is located in the islands. For realistic pit filling volumes (3.3 and 3.8 ML of Ge, see discussion above and blue stars and black squares in figure 11), the WL thickness between the pits drops for the field with $d_{pit} = 425$ nm even below 2 ML. This is remarkable, since a WL of 3 ML thickness is not yet in the 'thick-film limit' [53, 54]. If a WL is thinner than the thick-film limit, then adding a monolayer of Ge to the WL decreases its surface energy because the Ge atoms in the topmost layer are still influenced by the stronger bonds of the Si substrate beneath them [53, 54].

Consequently, when Ge from the WL surrounding the pit diffuses into the pits, the energetic benefit of decorating a pit with Ge and forming a Ge island in the pit must be comparable to the cost of the increasing surface energy of the WL with decreasing WL thickness (see [53]).

In figure 11 region I indicates where, with an increasing amount of Ge per unit cell, both island volume and WL thickness increase are favoured. In region II, the pyramid volumes saturate for $d_{pit} > 2\ \mu m^2$ at a value of about 5.5×10^4 nm^3. From [55] we know that close to this volume

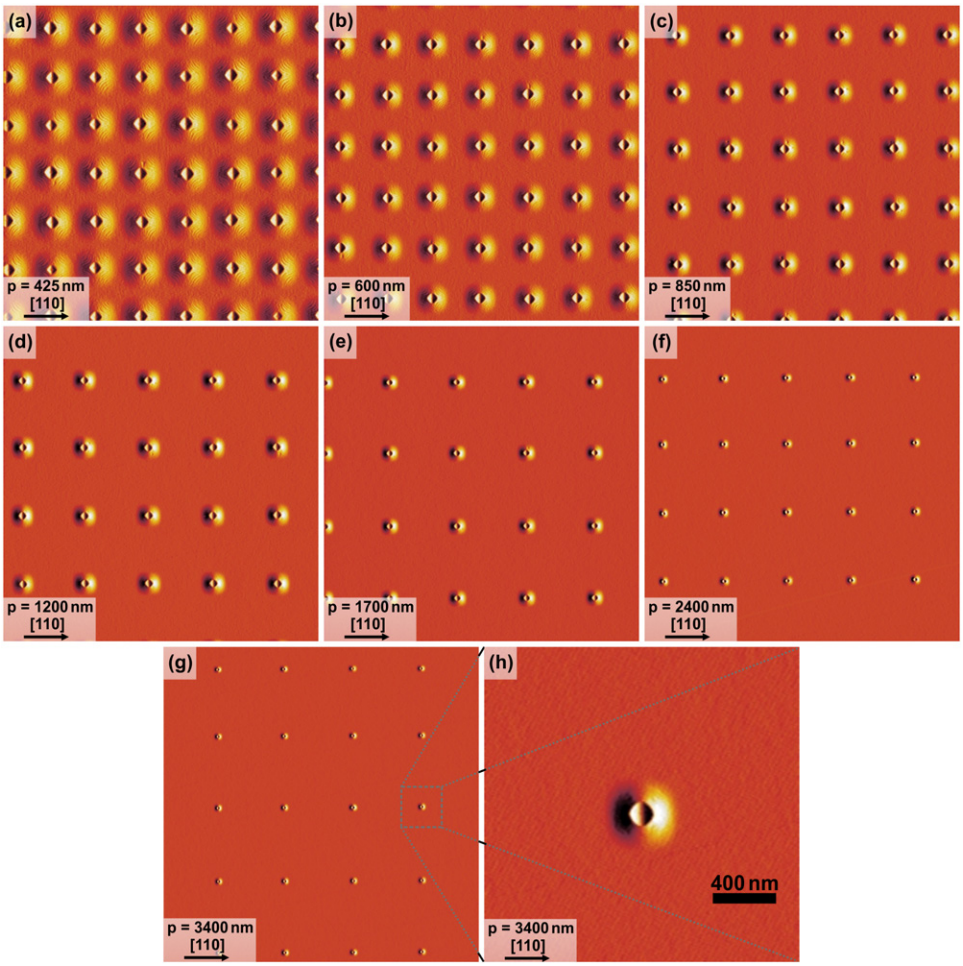

Figure 10. Strictly ordered islands on a single sample with wide d_{pit} variations. Sample template SG_B. AFM images in derivative mode of a sample (SG_B) after Si buffer layer growth and the deposition of 3 ML of Ge at 700 °C. d_{pit} increases from (a) 425 nm to (g) 3.4 μm. (h) presents a zoom-in of a pyramidal island in a field with $d_{pit} = 3.4$ μm. No secondary islands between the pits are observed.

pyramids transform on pit-patterned substrates into transition domes, i.e. islands that exhibit steeper {113}-facets at their apex in addition to the {105} pyramid facets [57, 58]. Creating a new facet initially increases the total energy [58, 64] because a few extra atoms on a reconstructed island facet correspond to a high surface energy configuration. Thus, creating a new island facet acts as an activation barrier for this morphological transition.

From this experimental evidence we interpret that this activation energy for the formation of a new facet cannot be overcome because WL thickening between the pits (up to 4.2 ML) is still favoured [53, 54] and thus the energetic cost of creating a new facet in combination with the increased surface energy at decreased WL thickness outweighs the benefit of the morphological island transition. In this case the WL acts as *stabilizer* that inhibits pyramids from undergoing a shape transformation to a dome-island through a metastable transition dome shape. Such an activation energy for the island's morphological transition as described above has to be expected whenever islands have to undergo a transition state where unfinished facets are present on the island's surface, e.g. at a transition from pyramids to domes, and also from domes to barns [65].

We can speculate how the growth would proceed if the deposition of Ge increased beyond the state presented in figure 10. Similar to the growth process described in [21], the WL would further thicken, lowering its surface energy. Depending on the ratio of Ge growth rate and island incorporation rate [55], either secondary island nucleation between the pits [21] or transformation of the pyramids in the pits into domes followed by a further morphological transition to bigger barns [11, 49] or dislocated superdomes [21] will occur. In an upcoming work [55] we will present a rate equation model quantitatively describing the influence of the Ge deposition rate on the morphological transitions of islands in pit-patterned Si(001) substrates.

4. Comparison to the InAs/GaAs system

As for Ge islands on Si substrates [1–24], also InAs dot site control was achieved on pit-patterned GaAs(001) substrates [66–74]. Many of the aspects of ordered Ge/Si island growth described in this work can also be helpful when applied to other material systems such as, for example, the InAs/GaAs system. The strain in the InAs/GaAs system

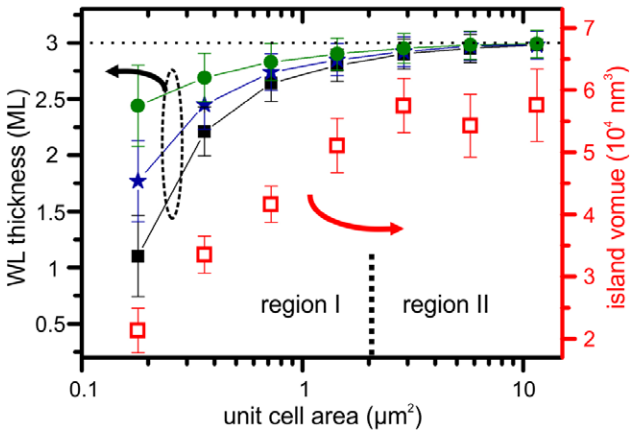

Figure 11. Island volume and WL thickness versus unit cell area, i.e. pattern period. Open red squares: pyramid volumes for different pit periods (425 nm–3.4 μm) (see figure 10) were evaluated for about 30 islands each period. The WL thickness between the pits was derived from the deposited Ge volume, the Ge volume stored in the islands and for three different volumes of Ge used for faceting the pit. Colour coded full symbols symbolize that 2.8 ML (green circles), 3.3 ML (blue stars) and 3.8 ML (black squares) of Ge are stored in the pits before the islands grow. The solid lines are guides for the eye. The dashed horizontal line indicates a WL thickness of 3 ML. I and II mark regions of monotonic island volume increase and constant island volume, respectively.

of 7.9% is significantly higher than in the Ge/Si system, where it amounts to 4.2%. Thus, the critical WL thickness for island nucleation is smaller (∼1.6 ML, [2]) for the InAs/GaAs system as compared to the approximately 4.2 ML for SiGe/Si(001) [51, 52].

Kiravittaya *et al* [2] have shown that there exist similarities between the two systems, despite the significantly different lattice mismatch of the constituent crystals. Depending on growth properties such as growth temperature and growth rate, a large variety of QD types exist in both systems, which can be easily distinguished by their surface faceting [2, 75]. Usually, the same architectonic names are given for those structures in the Ge/Si and InAs/GaAs systems, the most prominent being huts, pyramids, domes, barns and cupolas [2, 37, 56, 59, 65]. Shape transitions between the different island types are similar and well documented for both material systems [57, 58, 67] and the diffusion lengths of the adatom species (Ge or In and As, respectively) were found to be comparable (i.e. several micrometres) in both systems [63, 55, 67].

Additionally to those findings, it is important to mention that also the initially formed WL behaves in a similar way in the InAs/GaAs and Ge/Si systems. The influence of the WL thickness on the surface energy and chemical potential is very comparable. For both systems the first monolayer (ML) of the epilayer sticks very strongly to the substrate surface [54, 76] and the surface energy decreases with increasing WL thickness. This dependence of the surface energy on the WL thickness is in both material systems the reason for the formation of an In-rich [71] and a Ge-rich [77] WL which grows to an overcritical thickness (about one extra ML) [51, 52, 78]. The extra material stored in this metastable WL is used to form the initial islands, which are large dome islands [2, 51, 52].

The last two points, which seem to be minor effects for the growth of nanostructures, are actually of great importance when it comes to the growth of two-dimensional and three-dimensional arrays of QDs, see section 3.8. The loosely bound material stored in the WL, which will be transferred towards the material sinks in the pits [1], has to be taken into account if one is aiming at an ordered growth of dots.

Also the effect of GeSi and InAs–GaAs intermixing in the islands on the PL emission energies [17, 71] was found to be similar. In both GeSi and InAs islands the inhomogeneous Ge or In concentration leads to an enhanced confining potential that lowers the real electronic size of the islands below its geometrical size [17, 71].

5. Summary and conclusion

In summary, we have studied the strictly ordered growth of Ge islands on pit-patterned Si(001) substrates using MBE grown samples and post-growth AFM measurements. We presented an overview of the parameter space that has to be considered in order to obtain perfectly ordered islands. We have shown that already the pit preparation, i.e. the pit dimensions and the pit distance as well as the initially grown Si buffer layer, sets the course for successful Ge island growth. We find that the pit sidewall inclination after the Si buffer layer growth should be neither too low (>∼5°) nor too high (<∼18°). These angles represent the optimum pit sidewall inclination angle window for which highly symmetric islands grow at the centre of the pits.

Furthermore, the influence of the Ge growth rate, the amount of deposited Ge and the Ge growth temperature were addressed. We demonstrate that it is important to match these three parameters for a certain given pit period in order to avoid the formation of dislocated islands and secondary islands between the pits.

Finally, we presented a method to fabricate strictly ordered islands for a wide range of inter-pit distances. Our results highlight that the WL between the pits plays a crucial role in stabilizing the islands and thus allowing perfect ordering of Ge islands. We highlight that this is possible under the same growth conditions on one and the same sample, even if the pit period is varied from field to field from a few hundred nanometres to several micrometres.

Acknowledgments

This work was supported by the Austrian Science Funds (FWF): (SFB025-IRON, projects P02 and P12) and the Gesellschaft für Mikro- und Nanoelektronik (GMe). The authors would like to thank Günther Bauer for all his support.

Authors' contributions

MG and MB contributed equally to the work in designing the samples, carrying out the experiments, the statistical

analysis and writing the manuscript. GL fabricated a part of the substrate templates and contributed to their design. GL, TF and FS contributed to the manuscript layout. All authors discussed the manuscript.

References

[1] Schmidt O G (ed) 2007 *Lateral Alignment of Epitaxial Quantum Dots* (Berlin: Springer)

[2] Kiravittaya S, Rastelli A and Schmidt O G 2009 Advanced quantum dot configurations *Rep. Prog. Phys.* **72** 046502

[3] Berbezier I and Ronda A 2009 SiGe nanostructures *Surf. Sci. Rep.* **64** 47–98

[4] Karmous A, Fischer I A, Kirfel O, Mattes J, Oehme M, Werner J and Schulze J 2012 Recent developments in Ge dots grown on pit-patterned surfaces *Phys. Status Solidi* b **249** 764–72

[5] Kitajima T, Liu B and Leone S R 2002 Two-dimensional periodic alignment of self-assembled Ge islands on patterned Si(001) surfaces *Appl. Phys. Lett.* **80** 497–9

[6] Zhong Z-Y, Halilovic A, Fromherz T, Schäffler F and Bauer G 2003 Two-dimensional periodic positioning of self-assembled Ge islands on prepatterned Si(001) substrates *Appl. Phys. Lett.* **82** 4779–81

[7] Zhong Z Y and Bauer G 2004 Site-controlled and size-homogeneous Ge islands on prepatterned Si(001) substrates *Appl. Phys. Lett.* **84** 1922–4

[8] Karmous A, Cuenat A, Ronda A, Berbezier I, Atha S and Hull R 2004 Ge dot organization on Si substrates patterned by focused ion beam *Appl. Phys. Lett.* **85** 6401–3

[9] Zhong Z, Schmidt O G and Bauer G 2005 Increase of island density via formation of secondary ordered islands on pit-patterned Si(001) substrates *Appl. Phys. Lett.* **87** 133111

[10] Chen G, Lichtenberger H, Bauer G, Jantsch W and Schäffler F 2006 Initial stage of the two-dimensional to three-dimensional transition of a strained SiGe layer on a pit-patterned Si(001) template *Phys. Rev.* B **74** 035302

[11] Zhang J J, Stoffel M, Rastelli A, Schmidt O G, Jovanović V, Nanver L K and Bauer G 2007 SiGe growth on patterned Si(001) substrates: surface evolution and evidence of modified island coarsening *Appl. Phys. Lett.* **91** 173115

[12] Grützmacher D *et al* 2007 Three-dimensional Si/Ge quantum dot crystals *Nano Lett.* **7** 3150–6

[13] Zhong Z Y, Schwinger W, Schäffler F, Bauer G, Vastola G, Montalenti F and Miglio L 2007 Delayed plastic relaxation on patterned Si substrates: coherent SiGe pyramids with dominant {111} facets *Phys. Rev. Lett.* **98** 176102

[14] Schülli T U *et al* 2009 Enhanced relaxation and intermixing in Ge islands grown on pit-patterned Si(001) substrates *Phys. Rev. Lett.* **102** 025502

[15] Pezzoli F, Stoffel M, Merdzhanova T, Rastelli A and Schmidt O G 2009 Alloying and strain relaxation in SiGe islands grown on pit-patterned Si(001) substrates probed by nanotomography *Nanoscale Res. Lett.* **4** 1073–7

[16] Dais C, Mussler G, Sigg H, Müller E, Solak H H and Grützmacher D 2009 Evolution and stability of ordered SiGe islands grown on patterned Si(100) substrates *J. Appl. Phys.* **105** 122405

[17] Brehm M, Grydlik M, Hackl F, Lausecker E, Fromherz T and Bauer G 2010 Excitation intensity driven PL shifts of SiGe islands on patterned and planar Si(001) substrates: evidence for Ge-rich dots in islands *Nanoscale Res. Lett.* **5** 1868–72

[18] Grydlik M, Brehm M, Hackl F, Groiss H, Fromherz T, Schäffler F and Bauer G 2010 Inverted Ge islands in {111} faceted Si pits—a novel approach towards SiGe islands with higher aspect ratio *New J. Phys.* **12** 063002

[19] Vastola G, Grydlik M, Brehm M, Boioli F, Fromherz T, Bauer G, Montalenti F and Miglio L 2011 How pit facet inclination drives heteroepitaxial island positioning on patterned substrates *Phys. Rev.* B **84** 155415

[20] Zhang J J, Rastelli A, Schmidt O G and Bauer G 2011 Role of the wetting layer for the SiGe Stranski–Krastanow island growth on planar and pit-patterned substrates *Semicond. Sci. Technol.* **26** 014028

[21] Hackl F, Grydlik M, Brehm M, Groiss H, Schäffler F, Fromherz T and Bauer G 2011 Microphotoluminescence and perfect ordering of SiGe islands on pit-patterned Si(001) substrates *Nanotechnology* **22** 165302

[22] Boioli F, Gatti R, Grydlik M, Brehm M, Montalenti F and Miglio L 2011 Assessing the delay of plastic relaxation onset in SiGe islands grown on pit-patterned Si(001) substrates *Appl. Phys. Lett.* **99** 033106

[23] Sgarlata A, Persichetti L, Capasso A, Fanfoni M, Motta N and Balzarotti A 2011 Driving Ge island ordering on nanostructured Si surfaces *Nanosci. Nanotechnology Lett.* **3** 841–9

[24] Ma Y J, Zhong Z, Yang X J, Fan Y L and Jiang Z M 2013 Factors influencing epitaxial growth of three-dimensional Ge quantum dot crystals on pit-patterned Si substrate *Nanotechnology* **24** 015304

[25] Jovanović V *et al* 2010 n-channel MOSFETs fabricated on SiGe dots for strain-enhanced mobility *IEEE Electron Device Lett.* **31** 1083–5

[26] Katsaros G, Spathis P, Stoffel M, Fournel F, Mongillo M, Bouchiat V, Lefloch F, Rastelli A, Schmidt O G and De Franceschi S 2010 Hybrid superconductor–semiconductor devices made from self-assembled SiGe nanocrystals on silicon *Nature Nanotechnology* **5** 458–64

[27] Michler P, Kiraz A, Becher C, Schoenfeld W V, Petroff P M, Zhang L D, Hu E and Imanoglu A 2000 A quantum dot single-photon turnstile device *Science* **290** 2282–5

[28] Yuan Z, Kardynal B E, Stevenson R M, Shields A J, Lobo C J, Cooper K, Beattie N S, Ritchie D A and Pepper M 2002 Electrically driven single-photon source *Science* **295** 102–5

[29] Bouwmeester D, Ekert A and Zeilinger A 2000 *The Physics of Quantum Information* (Berlin: Springer)

[30] Takagahara T 1992 Quantum dot lattice and enhanced excitonic optical nonlinearity *Surf. Sci.* **267** 310–4

[31] Lazarenkova O L and Balandin A A 2002 Electron and phonon energy spectra in a three-dimensional regimented quantum dot superlattice *Phys. Rev.* B **66** 245319

[32] Aqua J-N, Berbezier I, Favre L, Frisch T and Ronda A 2013 Growth and self-organization of SiGe nanostructures *Phys. Rep.* **552** 59–189

[33] Politi P, Grenet G, Marty G, Ponchet A and Villain J 2000 Instabilities in crystal growth by atomic or molecular beams *Phys. Rep.* **324** 271–404

[34] Müller P and Saúl A 2004 Elastic effects on surface physics *Surf. Sci. Rep.* **54** 157–258

[35] Gray J L, Hull R and Floro J A 2002 Control of surface morphology through variation of growth rate in SiGe/Si(100) epitaxial films: nucleation of quantum fortresses *Appl. Phys. Lett.* **81** 2445–7

[36] Gray J L, Atha S, Hull R and Floro J A 2004 Hierarchical self-assembly of epitaxial semiconductor nanostructures *Nano Lett.* **4** 2447–50

[37] Brehm M, Lichtenberger H, Fromherz T and Springholz G 2011 Ultra-steep side facets in multi-faceted SiGe/Si(001) Stranski–Krastanow islands *Nanoscale Res. Lett.* **6** 70–8

[38] Robinson J T, Rastelli A, Schmidt O and Dubon O D 2009 Global faceting behavior of strained Ge islands on Si *Nanotechnology* **20** 085708

[39] Lichtenberger H, Mühlberger M and Schäffler F 2003 Transient-enhanced Si diffusion on native-oxide-covered

Si(001) nanostructures during vacuum annealing *Appl. Phys. Lett.* **82** 3650–2
[40] Rastelli A and von Känel H 2002 Surface evolution of faceted islands *Surf. Sci.* **515** L493–8
[41] Bergamaschini R, Tersoff J, Tu Y, Zhang J J, Bauer G and Montalenti F 2012 Anomalous smoothing preceding island formation during growth on patterned substrates *Phys. Rev. Lett.* **109** 156101
[42] Biasiol G, Gustafsson A, Leifer K and Kapon E 2002 Mechanisms of self-ordering in nonplanar epitaxy of semiconductor nanostructures *Phys. Rev.* B **65** 205306
[43] Huang L, Liu F and Gong X G 2004 Strain effect on adatom binding and diffusion in homo- and heteroepitaxies of Si and Ge on (001) Surfaces *Phys. Rev.* B **70** 155320
[44] Yang B, Liu F and Lagally M G 2004 Local strain-mediated chemical potential control of quantum dot self-organization in heteroepitaxy *Phys. Rev. Lett.* **2** 025502
[45] Hu H, Gao H and Liu F 2012 Quantitative model of heterogeneous nucleation and growth of SiGe quantum dot molecules *Phys. Rev. Lett.* **109** 106103
[46] Grydlik M, Brehm M and Schäffler F 2012 Morphological evolution of Ge/Si(001) quantum dot rings formed at the rim of wet-etched pits *Nanoscale Res. Lett.* **7** 601–6
[47] Kamins T I, Medeiros-Ribeiro G, Ohlberg D A A and Williams R S 1999 Evolution of Ge islands on Si(001) during annealing *J. Appl. Phys.* **85** 1159–71
[48] Dais C, Solak H H, Ekinci Y, Müller E, Sigg H and Grützmacher D 2007 Ge quantum dot molecules and crystals: preparation and properties *Surf. Sci.* **601** 2787–91
[49] Zhang J J *et al* 2012 Collective shape oscillations of SiGe islands on pit-patterned Si(001) substrates: a coherent-growth strategy enabled by self-regulated intermixing *Phys. Rev. Lett.* **105** 166102
[50] Matthews J W and Blakeslee A E 1974 Defects in epitaxial multilayers .1. Misfit dislocations *J. Cryst. Growth* **27** 118–25
[51] Brehm M *et al* 2009 Key role of the wetting layer in revealing the hidden path of Ge/Si(001) Stranski–Krastanow growth onset *Phys. Rev.* B **80** 205321
[52] Brehm M, Grydlik M, Groiss H, Hackl F, Schäffler F, Fromherz T and Bauer G 2011 The influence of a Si cap on self-organized SiGe islands and the underlying wetting layer *J. Appl. Phys.* **109** 123505
[53] Beck M J, van de Walle A and Asta M 2004 Surface energetics and structure of the Ge wetting layer on Si(100) *Phys. Rev.* B **70** 205337
[54] Lu G-H, Cuma M and Liu F 2005 First-principles study of strain stabilization of Ge(105) facet on Si(001) *Phys. Rev.* B **72** 125415
[55] Grydlik M, Brehm M, Hackl F and Fromherz T 2013 Unrolling the evolution kinetics of ordered SiGe islands via Ge surface diffusion *Phys. Rev.* B to be submitted
[56] Mo Y-W, Savage D E, Schwartzentruber B S and Lagally M G 1990 Kinetic Pathway in Stranski–Krastanov Growth of Ge on Si(001) *Phys. Rev. Lett.* **65** 1020–3
[57] Ross F M, Tromp R M and Reuter M C 1999 Transition states between pyramids and domes during Ge/Si island growth *Science* **286** 1931–4
[58] Montalenti F *et al* 2004 Atomic-scale pathway of the pyramid-to-dome transition during Ge Growth on Si(001) *Phys. Rev. Lett.* **93** 216102
[59] Medeiros-Ribeiro G, Bratkovski A M, Kamins T I, Ohlberg D A A and Williams R S 1998 Shape transition of germanium nanocrystals on a silicon (001) surface from pyramids to domes *Science* **279** 353–5
[60] Liao X Z, Zou J, Cockayne D J H, Wan J, Jiang Z M, Jin G and Wang K L 2002 Alloying, elemental enrichment, and interdiffusion during the growth of Ge(Si)/Si(001) quantum dots *Phys. Rev.* B **65** 153306
[61] Capellini G, De Seta M and Evangelisti F 2001 SiGe intermixing in Ge/Si(100) islands *Appl. Phys. Lett.* **78** 303–5
[62] Schmidt O G, Lange C and Eberl K 1999 Photoluminescence study of the initial stages of island formation for Ge pyramids/domes and hut clusters on Si(001) *Appl. Phys. Lett.* **75** 1905–7
[63] Kar G S, Kiravittaya S, Stoffel M and Schmidt O G 2004 Material distribution across the interface of random and ordered island arrays *Phys. Rev. Lett.* **93** 246103
[64] McKay M R, Venables J A and Drucker J 2008 Kinetically suppressed Ostwald ripening of Ge/Si(100) hut clusters *Phys. Rev. Lett.* **101** 216104
[65] Sutter E, Sutter P and Bernard J E 2004 Extended shape evolution of low mismatch $Si_{1-x}Ge_x$ alloy islands on Si(100) *Appl. Phys. Lett.* **84** 2262–4
[66] Heidemeyer H, Müller C and Schmidt O G 2004 Highly ordered arrays of In(Ga)As quantum dots on patterned GaAs (0 0 1) substrates *J. Cryst. Growth* **261** 444–9
[67] Kiravittaya S, Rastelli A and Schmidt O G 2005 Self-assembled InAs quantum dots on patterned GaAs(001) substrates: formation and shape evolution *Appl. Phys. Lett.* **87** 243112
[68] Atkinson P, Ward M B, Bremner S P, Anderson D, Farrow T, Jones G A C, Shields A J and Ritchie D A 2006 Site-control of InAs quantum dots using *ex situ* electron-beam lithographic patterning of GaAs substrates *Japan. J. Appl. Phys.* **45** 2519–21
[69] Lee J Y, Noordhoek M J, Smereka P, McKay H and Millunchick J M 2009 Filling of hole arrays with InAs quantum dots *Nanotechnology* **20** 285305
[70] Schneider C *et al* 2009 Single site-controlled In(Ga)As/GaAs quantum dots: growth, properties and device integration *Nanotechnology* **20** 434012
[71] Biasiol G, Barabwal V, Heun S, Prasciolu M, Tormen M, Locatelli A, Mentes T O, Nino M A and Sorba L 2011 Composition uniformity of site-controlled InAs/GaAs quantum dots *J. Cryst. Growth* **323** 176–9
[72] Cheng C-C, Meneou K and Cheng K Y 2010 Molecular-beam epitaxy growth of site-controlled InAs/GaAs quantum dots defined by soft photocurable nanoimprint lithography *J. Vac. Sci. Technol.* B **28** C337–40
[73] Skiba-Szymanska J *et al* 2011 Narrow emission linewidths of positioned InAs quantum dots grown on pre-patterned GaAs(100) substrates *Nanotechnology* **22** 065302
[74] Schramm A, Tommila J, Strelow C, Hakkarainen T V, Tukiainen A, Dumitrescu M, Mews A, Kipp T and Guina M 2012 Large array of single, site-controlled InAs quantum dots fabricated by UV-nanoimprint lithography and molecular beam epitaxy *Nanotechnology* **23** 175701
[75] Stangl J, Holý V and Bauer G 2004 Structural properties of self-organized semiconductor nanostructures *Rev. Mod. Phys.* **76** 725–83
[76] Wang L G, Kratzer P, Scheffler M and Moll N 1999 Formation and stability of self-assembled coherent islands in highly mismatched heteroepitaxy *Phys. Rev. Lett.* **82** 4042–5
[77] Brehm M, Grydlik M, Lichtenberger H, Fromherz T, Hrauda N, Jantsch W, Schäffler F and Bauer G 2008 Quantitative determination of Ge profiles across SiGe wetting layers on Si(001) *Appl. Phys. Lett.* **93** 121901
[78] Placidi E, Arciprete F, Sessi V, Fanfoni M, Patella F and Balzarotti A 2005 Step erosion during nucleation of InAs/GaAs(001) quantum dots *Appl. Phys. Lett.* **86** 241913